

Continuous roll-to-roll fabrication of transparent cellulose nanocrystal (CNC) coatings with controlled anisotropy

Reaz A. Chowdhury  · Caitlyn Clarkson · Jeffrey Youngblood

Received: 5 September 2017 / Accepted: 30 January 2018 / Published online: 5 February 2018
© Springer Science+Business Media B.V., part of Springer Nature 2018

Abstract Cellulose nanocrystals (CNCs) can impart desirable barrier properties in film packaging applications; however, commercial production of these materials is inhibited by the absence of a large-scale manufacturing process for producing CNC coatings. To fill this knowledge gap, a potential large-scale manufacturing process, roll-to-roll gravure printing, for cellulose nanocrystal coating on a flexible polyethylene terephthalate substrate has been described in this work. Processing parameters which control the coating structure and properties were examined. For a given gravure roll, gravure speed, substrate speed, and ink viscosity were determined to be the most important parameters that control the liquid transfer from the ink bath to the substrate, which determined the coating thickness (2–6 μm). After successful fabrication, CNC coating adhesion was investigated with a cross-hatch adhesion test. The adhesive strength of the CNC coating was correlated with coating thickness, and the maximum coating strength was observed for the lowest coating thickness. Coatings were characterized using atomic force microscopy and UV–Vis

spectroscopy. Finally, the crystalline domain arrangement of coatings was determined for coatings made from three different CNC concentrations, and the effect of viscosity on CNC alignment was explained by variation of shear rate, which was controlled by the micro-gravure rotation.

Keywords Gravure · Cellulose nanocrystal · Roll-to-roll · Anisotropy · Transparency

Introduction

Cellulose nanocrystals (CNCs) are an alternative renewable material derived from abundant resources: wood, plants, algae, tunicate, bacteria, etc. CNCs have a rod-shaped anisotropic crystalline domain with excellent properties, such as non-toxicity, biodegradability, high specific strength, high thermal conductivity, and optical transparency (Diaz et al. 2014; Isogai et al. 2011; Moon et al. 2011). Based on these remarkable properties, CNCs are applicable as a reinforcement component in nanocomposites (Liu et al. 2015; Peng et al. 2014; Yoo et al. 2017), transparent media in organic electronics (Zhou et al. 2014), anti-counterfeiting in security applications (Chindawong and Johannsmann 2014), and barriers in packaging applications (Lavoine et al. 2012). CNCs can form a coating (Yoo and Youngblood 2017), film

Electronic supplementary material The online version of this article (<https://doi.org/10.1007/s10570-018-1688-4>) contains supplementary material, which is available to authorized users.

R. A. Chowdhury · C. Clarkson · J. Youngblood (✉)
School of Materials Engineering, Purdue University,
West Lafayette, IN 47907, USA
e-mail: jpyoungb@purdue.edu

(Reising et al. 2012), aerogel (Yang and Cranston 2014) or foam (Dong and Snyder 2013) depending on the desired final application.

The mechanical, thermal and optical properties of CNC materials depend significantly on the structural arrangement of the crystalline domain (Chen et al. 2014; Chowdhury et al. 2017; Diaz et al. 2013; Reising et al. 2012; Wicklein et al. 2015). Depending on the crystal domain organization, CNC materials can be isotropic or anisotropic where an anisotropic configuration can exhibit directional enhanced properties in the orientation direction. For example, a four-fold higher thermal conductivity in the aligned direction compared to the isotropic configuration has been reported (Diaz et al. 2014). Anisotropic CNC nanocomposites can offer better properties such as higher Young's elastic modulus, yield stress, and ultimate tensile strength with improved transparency, which is essential for gas barrier application (Kalia et al. 2011). Anisotropic CNC film also presents exceptionally low hygroscopic strain in the axial direction that is important for any electronic packaging application (Shrestha et al. 2017).

Solution casting using mechanical shear force is the most common technique for anisotropic CNC film fabrication (Chowdhury et al. 2017; Haywood and Davis 2017; Orts et al. 1998; Park et al. 2014; Reising et al. 2012). Solution casting is a convenient and inexpensive small-scale processing technique, however high viscosity solutions are primarily used. High concentrations of CNC (and thus high viscosity solutions) allow for limited mobility of the CNCs during processing and therefore, the coating retains shear-induced anisotropy in its final structure. However, difficulties exist in achieving a uniform homogeneous thickness and the fabrication process is time consuming for such solutions (an hour to several days). Spin-coating overcomes this limitation, but large area processing is a challenge for this method (Cranston and Gray 2008). In this context, roll-to-roll manufacturing offers an inexpensive, fast process with large-scale continuous fabrication compared to other laboratory-scale processing techniques.

The roll-to-roll (R2R) manufacturing process is a versatile technique for the fabrication of flexible coatings, polymer solar cells, and flexible electronic devices (Ahn and Guo 2008; Bae et al. 2010; Galagan et al. 2011; Krebs 2009; Krebs et al. 2009; Lewis and Paine 2000; S ndergaard et al. 2013). Both printing

and coating are possible in a roll-to-roll system, which can be coupled with slot-die, gravure, spray, inkjet, nanoimprinting, or rotary screen. In an R2R gravure process, ink is continuously transferred from an ink bath to the gravure cylinder. A doctor blade is placed over the gravure cylinder to remove the excess ink and maintain a constant uniform ink thickness. A thermoplastic, flexible polymer film is used as a substrate, which continuously moves between the two rolls. A liquid bridge between the gravure cavity and the web (substrate) that is stretched and sheared with a moving contact line is the basic mechanism of the ink transfer from the gravure to the web. Typically, the wet liquid film then passes through a drying chamber and dries. The overall coating quality largely depends on the ink's compatibility with the substrate, gravure speed rate, web speed, drying unit, and solvent type. Gravure coating has been used to fabricate organic thin film transistors, light-emitting polymer diodes, organic photovoltaics, and electrochromic devices (S ndergaard et al. 2013).

Very limited work has been done using R2R with cellulose nanomaterials. Previous studies focused on pure CNF and CNF mixtures for thin or thick coating formations (Kumar et al. 2016; Rantanen et al. 2015). To the best of our knowledge, R2R micro-gravure has never been used for CNC based coatings. Accordingly, we use micro-gravure R2R to develop and report an industrial scale, anisotropic CNC film coating technique on a flexible PET substrate. In this work, we detail the role of process parameters such as roller speed, web speed, and viscosity on the coatings and report the effect of gravure rotation rate on the coating thickness and anisotropy.

Experiments

Materials and ink formulation

Flexible polyester films (MELINEX[®] 462 2 mil) were purchased from TEKRA (New Berlin, WI, USA) and used as a substrate. The substrate–film, 1000 m in length and 15.24 cm in width, was installed on the roll-to-roll coating system. Never-dried, pristine CNC (12.2 wt%, batch no-2015-FPL-071CNC) aqueous suspension purchased from the University of Maine (Orono, ME, USA) and manufactured by the USDA Forest Service-Forest Products Laboratory (FPL)

(Madison, WI, USA), was used as ink in this investigation. The stock CNC aqueous solution was diluted with nano-pure water to a final concentration of 6, 9, and 12 wt% CNC. Henceforth the ink was referred to as the pristine CNC suspension. Solutions were ultra-sonicated (at 50% amplitude with 60 Hz frequency) for 10 min to disperse CNCs and homogenize solutions. Sonication introduced fluidity into solutions by destroying its gel structure and enabling their use as an active ink system without any further formulation. The rheological measurements of the CNC suspension were performed on a shear controlled rotational rheometer (Malvern Bohlin Gemini HR Nano) equipped with a cup and bob fixture. The steady shear viscosity was measured for 100 μm gap distance and the shear rate range was 0.01–500/s. All measurements were performed at room temperature.

Substrate and ink compatibility

Substrate-ink compatibility is the most important parameter for any printing or coating technique. In general, the surface energy of the substrate must be higher than the surface tension of the ink system. Flexible polyester films have lower surface energy (45 dynes/cm) compared to CNC dispersion surface tension (55–65 dynes/cm) (Gardner et al. 2008); hence, surface treatment is essential to overcome dewetting issue. Section 6 in the supporting information provides surface tension measurements for the three CNC suspensions (Figure S6). We utilized a high speed, high power corona treater system (QC electronics, Inc.) for substrate processing, which introduced a surface modification to increase the wettability of the substrate roll. Treatment speed rate as well as power supply dominated the overall surface modification. We observed that a substrate treatment with a 0.5 KW power supply and 2 m/min speed rate can produce 60–65 dynes/cm surface energy on the film, which is compatible with an aqueous CNC suspension.

Film fabrication

A Mirwec Mini-Labo DeluxeTM system (Figure S1) with a tri-helical R30-microgravure system (details in the supporting information, Section 7) has been utilized for our gravure coating. The gravure coating includes a gravure roller, ink bath, flexible substrate,

and drying chamber. A doctor blade was placed over the gravure cylinder to remove the excess ink and maintain a uniformly solution thickness. The nip distance was minimized between the gravure and the substrate to achieve complete liquid transfer. Fabrication processes were performed with a variable substrate speed (0.3–6 m/min), and gravure speed (4–70 rpm), which controlled the overall coating thickness and quality. After a successful liquid transfer from the ink bath to the flexible substrate, the wet-coated region passed through an inline drying unit. The temperature of the heating chamber was 80 °C for the entire gravure coating process, which allows for complete drying of the coating. After drying, the transparent CNC coated substrate was collected on the rewinder.

Film characterization

A Carl Zeiss (Axio observer A1) inverted light microscope was used in transmission mode for thickness measurements. Both 5X and 10X magnification objectives were used for film thickness characterization. A cut sample was placed perpendicularly between the objective and the stage and film thickness was measured. Polarized light optical microscopy was used to image coatings with samples at 45° and 90° with respect to the plane of polarized light.

The transparency of neat PET and CNC coated PET films were measured with a conventional UV–Vis spectrophotometer (Spectramax Plus 384, Molecular devices Corp., Sunnyvale, CA). The transmittance data for each film were measured across 400–750 nm wavelength with air as the background.

Adhesion test

CNC coating adhesion to the flexible substrate was studied with a cross-hatch adhesion test method (ASTM-D3359). Briefly, a 5X5 cm specimen was adhered to a glass plate with adhesive spray and left untouched for 30 min for complete drying. With a sharp blade, 11 parallel and 11 perpendicular cuts were made on the sample with respect to the center of the film, where each cut was 1 mm apart. A pressure sensitive tape was placed over the film for 5 min and removed from the surface at a 180° angle. The quantification of the adhesion loss via coating performance was categorized on a scale of 0–100%. Based

on the ASTM D3359, samples were classified into 6 different categories as follows: 5B (0%), 4B (less than 5%), 3B (5–15%), 2B (15–35%), 1B (35–65%) and 0B (> 65%) where 5B is considered optimal with 0% area removed from the substrate. Both the flexible substrate and CNC coating were colorless, so the removal of the CNC coating from the grid area was investigated by polarized light microscopy.

Surface morphology

A Dimension 5000 Atomic force microscope (AFM) in tapping mode was used to examine surfaces of organic coatings on the polyester substrate. Inspire CT300R-25 conical cantilever AFM tips were purchased for film characterization from NanoScience Instruments, Phoenix, AZ, USA. Samples were prepared by cutting a section of the film from the middle of the coated section and adhering the strip to a metal puck. Two samples were selected for each condition (6, 9, and 12 wt%) and three sections of $50\ \mu\text{m} \times 50\ \mu\text{m}$ on each sample imaged. Films were fabricated under the same conditions at a speed ratio of 1. Films for AFM imaging showed no visual signs of microscopic defects when viewed under an optical microscope.

Anisotropy measurement

A conventional UV–Vis spectrophotometer (Spectra-max Plus 384, Molecular devices Corp., Sunnyvale, CA) was used for the characterization of the CNC alignment. We used a similar method as reported by Chowdhury et al. and details can be found there (Chowdhury et al. 2017). Briefly, a sample was delaminated from the substrate and placed between a cross polarizer and the transmitted light intensity was measured at 45° and 90° configurations. The transmittance data was recorded from 400 to 750 nm wavelength. The following equations were used for the order parameter, S calculation:

$$I_\theta = I_0 \sin^2 2\theta \sin^2 \left(\frac{\pi \Delta n d}{\lambda} \right) \quad (1)$$

Hence,

$$\frac{I_{45}}{I_{90}} = D^* = D \cdot g = \frac{(2S + 1)}{(1 - S)} \quad (2)$$

Here, I_0 , θ , Δn , d , λ , I , g and D represent the amplitude of the incident light, the angle of the material between the cross-polarizer, refractive index difference, film thickness, wavelength, transmitted light intensity, correction factor and dichroic ratio, respectively. The parallel and perpendicular refractive indices are relatively low for cellulose; therefore, we adopt $g = 1$ for our calculation. The order parameter for any material is between 0 and 1, where $S = 0$ is defined as an entirely random/isotropic configuration and $S = 1$ is for a perfect anisotropic arrangement.

Results and discussion

Coating thickness control

Parameters such as micro-gravure speed, substrate speed, speed ratio, capillary number, and CNC concentration collectively control the liquid transfer rate of this fabrication process. A thick liquid layer is the first requirement for maximum liquid transfer from the gravure to the substrate. The liquid thickness solely depends on a stable and continuous liquid bridge formation between the gravure and substrate. However, stretching and shear forces also exist in this liquid bridge which can destabilize it; these forces can be controlled by gravure roller and web speeds (Kumar 2015). A table of the coating thickness dependence on experimental parameters is presented in the supporting information section 1 for each CNC concentration examined.

At a constant web speed, coating thickness increases with increasing roller speed and increasing CNC concentration, as shown in Fig. 1. By doubling the CNC concentration from 6 to 12 wt% the coating thickness approximately doubled for roller speeds less than 4 m/min. Similarly, the 9 wt% is approximately 1.5 times greater than the 6 wt% coatings. For these conditions, solid loading of the CNC nanoparticles in the ink (i.e. concentration) primarily controls coating thickness. However, the viscosity, and therefore capillary number, which increases monotonically with viscosity, are also expected to contribute to coating thickness as these parameters should theoretically improve the liquid transfer rate (Dodds et al. 2009, 2011; Patel and Benkreira 1991). At higher roller speeds, the capillary number for 12 wt% is 12

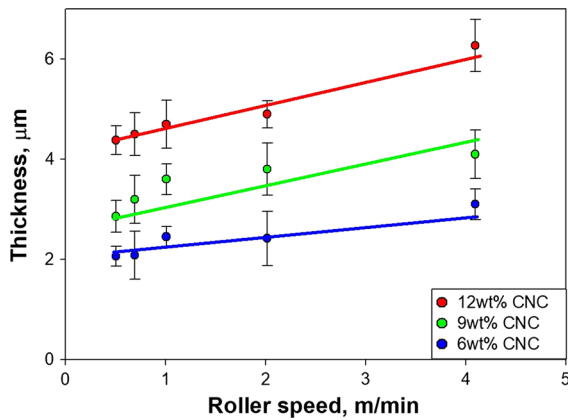


Fig. 1 The effect of roller speed for a constant web speed (1 m/min) (line added to aid the eye)

times higher than 6 wt% CNC suspensions, and coating thicknesses greater than twice the 6 wt% coatings were achieved. At the higher roller speeds, the increase in thickness may be owing to the significant increase in capillary number and hence better liquid transfer rate from the roller to the substrate. While the 9 wt% concentration followed a similar liquid transfer behavior to the 12 wt% CNC suspension, the 6 wt% CNC displayed the lowest capillary numbers for this system; hence, the liquid ink exhibits Newtonian behavior and follows a symmetrical liquid bridge breakup (Hewson et al. 2011; Huang et al. 2008). Consequently, a Newtonian liquid cannot de-wet completely from the gravure cell cavity resulting in low ink transfer and therefore, low coating thickness.

On the other hand, constant roller rotation with a variable web speed demonstrates the opposite behavior due to the reduced liquid transfer rate (Fig. 2). At a low web speed, the roller can rotate more than one time over the web surface resulting in the maximum coating thickness at low web speeds. However, liquid transfer rate reduces gradually with increasing web speed, therefore lowering the coating thickness. In general, the direction of the stretching force should be along the web direction, and the inertia force of the liquid will be along the roller direction. Both are altered by changing the web speed. At higher web speed, the inertia force dominates the stretching force, which facilitates a lower liquid transfer rate to the web surface. For variable web speed, increasing concentration from 6 to 9 wt% and 12 wt% did not produce coatings with respective thickness 1.5–2 times greater,

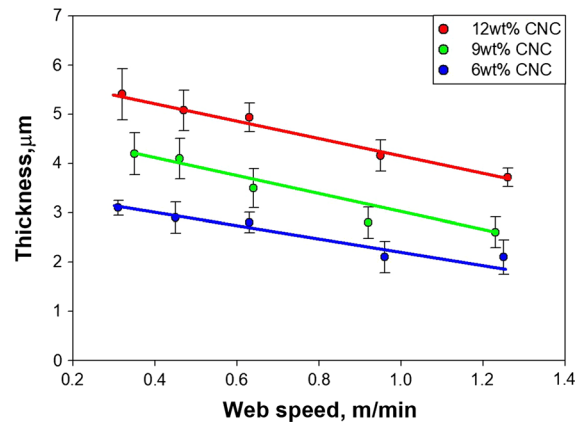


Fig. 2 The effect of web speed for a constant roller speed (0.63 m/min) (line added to aid the eye)

therefore, viscous and inertia forces played a role in liquid deposition. However, these effects are still small relative to solids loading.

The speed ratio is a critical parameter dependent upon on the roller and substrate speeds, where the capillary number of the liquid suspension controls the liquid transfer rate for the fabrication process. The thickness of the resultant films, and therefore liquid transfer rate from the ink bath to the substrate, increased by a small amount with increasing speed ratio for all CNC concentrations as shown in Fig. 3. Per Hewson et al., the data was fit to a 2-parameter rectangular hyperbola (Hewson et al. 2010, 2011; Kapur 2003). The liquid transfer rate also depends on the viscous force and inertia force where viscous

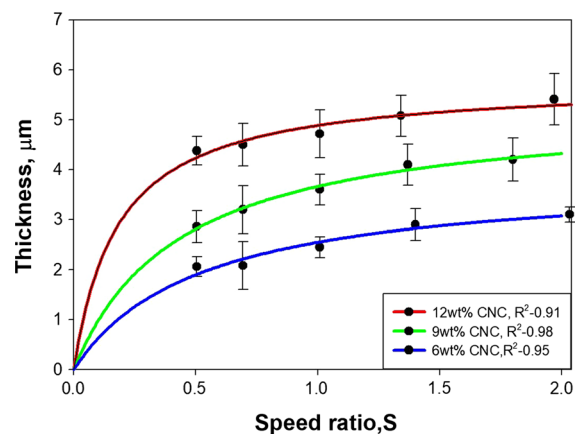


Fig. 3 The effect of speed ratio on the coating thickness for three CNC suspensions (nonlinear regression based on 2 parameter rectangular hyperbola)

forces must dominate the inertia force to increase the coating thickness. At a lower speed ratio (0–0.5), the viscosity of the 12 wt% CNC suspension is very high compared to the other concentrations. So, liquid transfer rate must be higher for the 12 wt% suspension based on capillary number alone. Similarly, 9 wt% has a higher viscous force compared to the 6 wt% suspension and resulted in a higher transfer rate and overall higher coating thickness than the lowest concentration. Due to the extremely shear thinning nature of CNC dispersions, increasing shear rate (governed by increasing gravure rotation) will reduce ink viscosity significantly (Fig. 4), which will reduce the liquid transfer rate at the higher speed ratio region. At this reduced viscosity, all CNC concentrations behave as Newtonian fluids in which symmetrical liquid bridge formation is the liquid transfer mechanism. Moreover, in the high-speed ratio region, the capillary number is also reduced because of the reduction in suspension viscosity at high shear rates, see Fig. 4. The reduction of the capillary number and symmetrical liquid bridge formation are the primary reasons for steady state liquid transfer at high speed ratios where the sample thickness begins to asymptote for all suspensions (Fig. 3).

We developed 3D mesh plots with corresponding contour plots for coating thickness as a function of web speed and gravure rotation. The highest concentration suspension shows a wider region of coating thickness with increased gravure rotation compared to the 6 and 9 wt% counterparts in Fig. 5. Speed ratios from 2 to 3.2 show a highly defected coating and so are of limited utility (Figure S2). However, defect-free

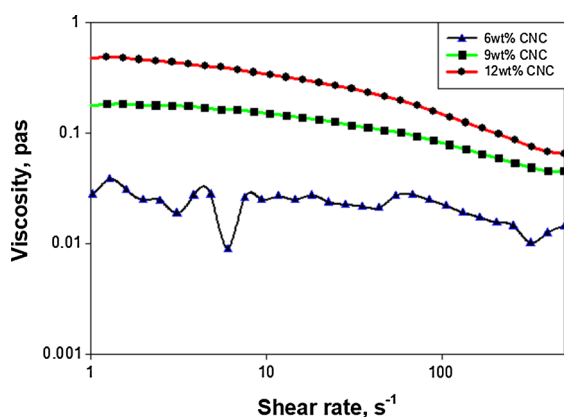


Fig. 4 Rheological properties of 12, 9 and 6 wt% CNC suspensions

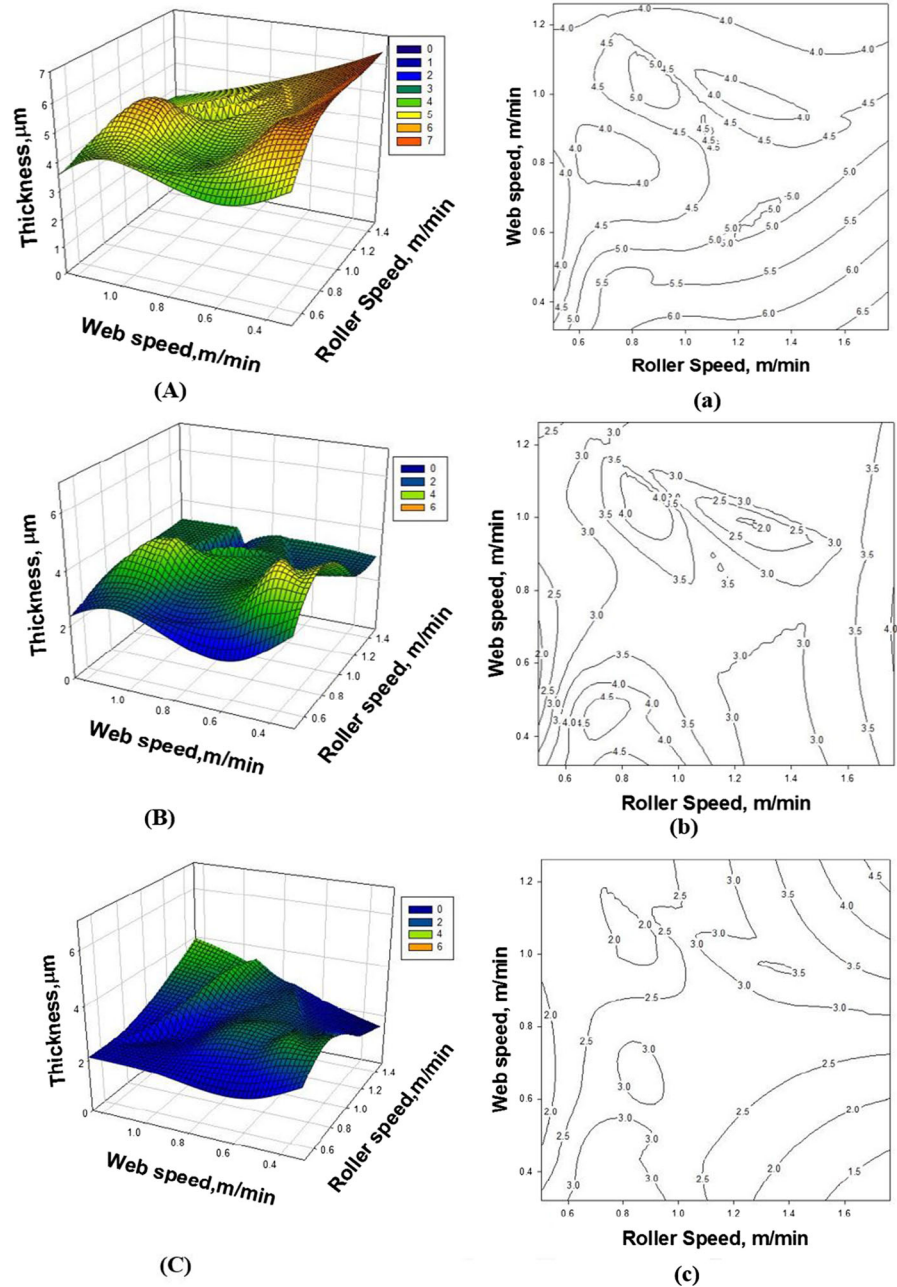
coatings with reduced thickness were observed at lower speed ratios and higher web speeds. The 9 wt% CNC suspension shows a much smaller region for the thickest coatings with slow gravure rotation. It appears that the maximum liquid transfer rate can be attributed to higher viscosity ink systems. We did not identify any significant effect on coating thickness for 6 wt% CNC suspension which may be a consequence of the solution exhibiting a very low capillary number and Newtonian like liquid properties. Moreover, Newtonian-like liquids exhibit symmetrical liquid bridge breakup, where the symmetrical liquid bridge breakup is always independent of viscosity, roller, and web speed effects, resulting in a constant liquid transfer from the roller to the web surface (Kumar 2015).

A balance between CNC concentration, roller speed, and web speed was obtained to achieve defect free coatings. Higher CNC concentrations are desirable as larger thicknesses are readily produced and shear induced anisotropy (which will be discussed later) is preserved as CNCs at high concentrations are less mobile. However, high concentration can prohibit entrapped air from escaping the solution and prevent the relaxation of the solution, which can manifest as defects in the dried coating. Likewise, fast roller speeds and slow web speeds result in multiple rotations of the roller across the substrate surface and produces a thicker coating. Although increasing web speed may be desirable for increasing production rate, at very high web speeds non-uniform coatings are produced with pinhole defects (Figure S2). At higher speed ratios where the web speed is less than roller speed, defects induced were de-wetting of the suspension due to bubble formation and line defects attributed to the Marangoni effect (Figure S2).

Effect of film thickness on coating adhesion

Samples of various coating thicknesses were subjected to crosshatch adhesion tests to measure coating adhesion. Adhesive bonding within the coating and at the coating-substrate interface varies with the coating thickness. Since visual inspection of debonding on transparent coated PET film was challenging; polarized light was used to quantify the adhesion loss of CNC coatings (Figure S3). Samples were illuminated between crossed polarizers, and the damaged area was identified based on the color contrast. The coating array before and after the

Fig. 5 3D mesh plot with corresponding contour plot for 12 wt% (A–a), 9 wt% (B–b), and 6 wt% (C–c) CNC coating



crosshatch test can be seen in Figure S4 of the supporting information.

CNC coatings exhibit high peel strength from the PET substrate. Substrate-coating interaction plays a significant role in the peeling strength and is determined by the surface energy and surface tension of the substrate and ink (CNC dispersion in water), respectively. Hence, a highly wettable coating shows very

strong adhesion (Kendall 1971). Corona or plasma treated PET substrates, which have a higher surface energy and therefore are more wettable, show much higher adhesive strength compared to untreated PET substrates (Lerouge et al. 2015). A similar behavior was also observed for the crosshatch experiments here since a corona treatment was applied to the PET substrate.

Coating adhesion displays a strong dependence on coating thickness despite lowering the surface energy difference at the interface through surface treatment. The total coating thickness from 6 wt% CNC suspension was between 2–3 μm , and no delamination was observed for this coating thickness range (Fig. 6). Increasing the CNC concentration to 9 wt% CNC suspension increases the final coating thickness to 3.5–4.5 μm and coincides with the onset of delamination in the adhesion test of coated films and therefore a decrease in coating performance. Furthermore, CNC coatings produced with the 12 wt% CNC suspension (4.5–6 μm total thickness) demonstrate the lowest adhesive rating compared to 6 and 9 wt% suspension. Conceivably a variety of factors could be leading to the higher adhesion of thinner layers. However, it is observed that the coating adhesive strength on PET substrate is independent of the initial ink concentration. To test this observation, a 2–3 μm thick CNC coating from 12 wt% CNC suspension was prepared with a R180 microgravure, and a crosshatch adhesion test was performed. No significant delamination was observed which confirm that adhesion is independent of initial CNC concentration.

The cohesive strength of the bulk CNC coating, and the adhesive strength between the substrate-coating interfaces can explain the above observation. As a rule of thumb, a reduced coating thickness can improve coating adhesion (Chiang et al. 2005). As the final coating thickness depends on the initial CNC concentration, the thinnest coatings produced by the 6 wt% suspension possessed the maximum peel strength

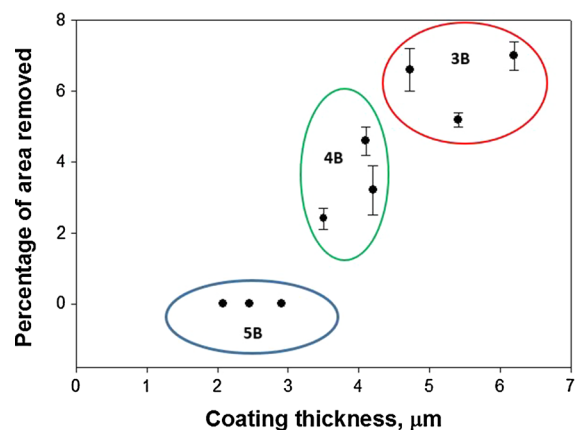


Fig. 6 Crosshatch peel adhesion strength of 12, 9 and 6 wt% at varying coating thickness

(Fig. 6). Theoretically, the cohesive strength should not change significantly for any thickness difference; moreover, the adhesive strength at the interface is independent of the coating thickness. We expected the adhesive rating to be similar for all CNC concentrations, but, we observed delamination for 9 and 12 wt% CNC suspension based coating. Fabrication defects present on the surface and in bulk coating regions, which strongly depend on film thickness, may initiate cracks in the coating that result in delamination. As well, there may be residual stress in the films owing to their rapid drying and low solids gel point (Moon et al. 2011).

The mechanism of defect formation in roll-to-roll system strongly depends on the viscosity and capillary number of the ink system. Here, high viscosity liquids (9 and 12 wt%) will have higher capillary numbers. Higher capillary number fluids can entrap air bubbles on the gravure, which can lead to different coating defects (see Figure S2 in the supporting information). Moreover, high-speed gravure rotation of a viscous ink system can also produce air bubbles in the ink bath which in turn may produce defects in thicker coating samples not present in thinner coatings. The presence of a volume defect like cavitation can reduce the adhesive bond between the interfaces and therefore reduce the adhesive strength which results in delamination or de-bonding at higher coating thicknesses.

Effect of CNC concentration on surface morphology and optical transparency

Surface morphology varied greatly with CNC concentration. As CNC concentration was increased, the surface roughness was seen to increase, see Fig. 7. Both the 9 and 12 wt% surface morphologies were considerably rougher compared to the 6 wt% suspension, which is reflected in R_q , the root mean squared height deviation, of Table 1. The presence of groove or current-like morphologies in the 9 wt% indicate a strong directional dependence of the surface morphology. The direction of the grooves approximately coincides with the 0° – 20° orientation introduced by the gravure tilt along the direction of shear. For highly viscous suspensions like the 9 and 12 wt% the relaxation time is longer and so solutions will retain more orientation during processing, as seen with the order parameter in the subsequent section, in the rolling direction. The scale and frequency of this

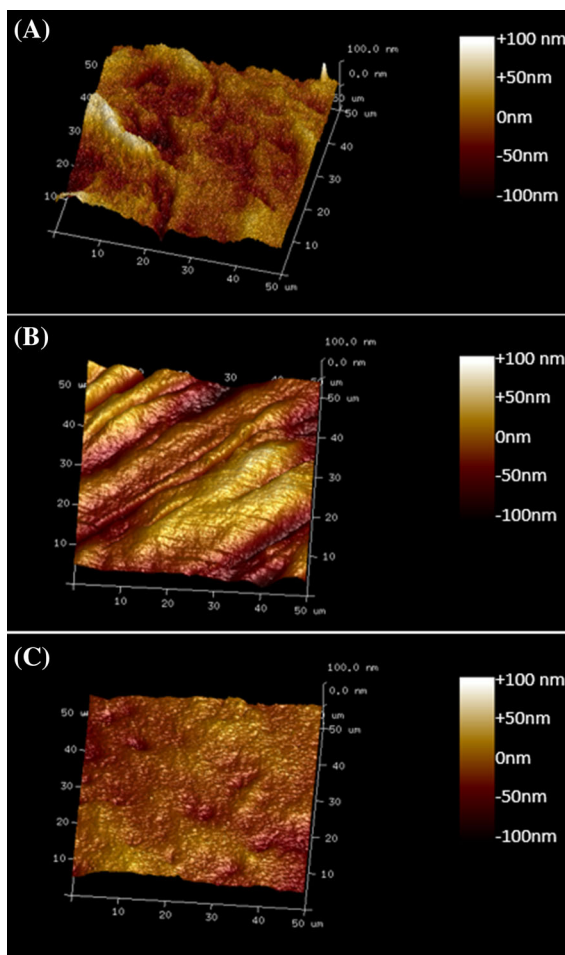


Fig. 7 Surface morphologies of coatings from suspensions of **a** 12 wt% CNC, **b** 9 wt%, and **c** 6 wt%

Table 1 Roughness measurements as a function of CNC content

CNC content (wt%)	R_q (nm)	R_{max} (nm)
12	14.4 ± 1.08	126 ± 28.47
9	18.11 ± 3.58	139 ± 20.00
6	6.39 ± 0.77	65.27 ± 7.52

R_q : root mean squared deviation in height

R_{max} = maximum vertical height difference

morphology are both too small to be gravure patterning. The unique appearance may be a result of local dewetting of the suspension from the surface similar to microscale defects seen at higher speed ratios. While the 12 wt% is still rough, it did not exhibit a strong direction dependence did in the areas examined. It did

have several pockets, which may be the result of cavitation (Figure S2). Cavitation can occur when air becomes entrapped in a viscous solution and is transferred to the surface. The 6 wt% exhibited small variation in sample roughness, see Table 1. This is not surprising as the suspension behaved as a Newtonian fluid and has a fast relaxation time compared to the 9 and 12 wt%, see Figure S5. In particular, the maximum vertical height difference, R_{max} , and R_q were proximately twice as large for the 9 and 12 wt% CNC coatings compared to the 6 wt%. Increased surface roughness creates a stronger adhesive bond between the coating and the tape in the peel test by strengthening the mechanical bond between the surface and tape. Increased surface roughness can be problematic as defects and uneven surfaces are sites for failure. The increased roughness of the higher suspensions may be one reason the 9 and 12 wt% adhesion performance was so low compared to the 6 wt%.

Surface morphology is indicative of the liquid transfer efficiency as well. A liquid bridge exists between the gravure and the substrate in which ink is transferred. Across this liquid bridge there can be a surface tension gradient which will help drive liquid transfer. If the surface tension of the liquid is minimized by wetting the substrate, it will do so. A reasonable expectation is that the surface morphology would be smooth and flat if surface tension favors the transfer of the ink to the substrate. However, viscous forces will be competing against surface tension. As the viscosity of the liquid increases the capillary number increases. For high viscosity, high Ca, the viscous forces will dominate surface tension effects in flow behavior and the surface may still appear rough despite liquid transfer being a favorable process. In the present study, the capillary number is increasing with increasing CNC concentration which may explain why surface roughness is increasing significantly despite favorable wetting conditions after corona treatment and layer-by-layer coating.

Exceptional optical transparency was obtained for CNC coated PET films (see Fig. 8). Flexible PET demonstrated 89–92% transparency for a wavelength range from 400 to 750 nm, while CNC coating transparency degraded only 2% compared to the bare substrate (Fig. 9). This reduction may be due to the differing refractive index of the CNC coatings or due to the higher surface roughness of the coatings compared to the substrate. Of the CNC coatings, the



Fig. 8 Photographs of CNC coatings on PET substrate (15 cm × 15 cm): (top left) PET substrate, (top right) 12 wt% CNC solution, (bottom left) 9 wt%, (bottom right) 6 wt%

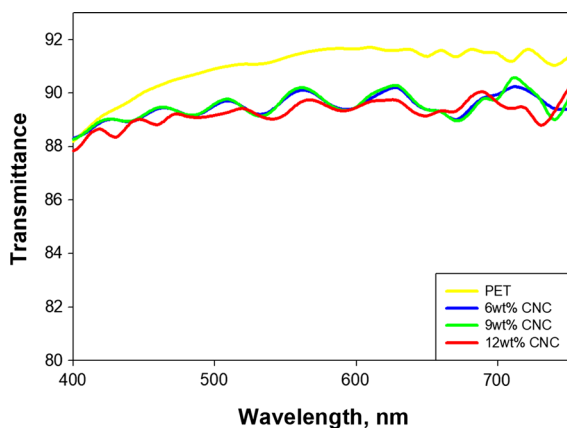


Fig. 9 Optical transparency for different CNC coated PET films

12 wt% transparency was 1.5% lower than the 6 and 9 wt%. The presence of defects (due to a higher capillary number and gravure rotation) or higher surface roughness in 12 wt% CNC coating may be responsible for the slight decrease. The diffuse reflection of incident light is promoted by surface roughness and may cause light scattering, reducing the

ultimate transparency of the 12 wt% film. Moreover, edges of defects can cause diffraction of the incident light and therefore also; reduction of transparency. Regardless, all transparency loss of the coatings is small and not noticeable by the naked eye.

Gravure rotational effect on anisotropy (nematic configuration)

The liquid crystal domain arrangement (anisotropy, in this case) is largely determined by the combined action of the shear rate and domain retention time, which depends on the gravure rotation and the rheology of the CNC solution. To calculate Herman's order parameter, S , light transmittance of free-standing CNC films was measured. Films were created by varying gravure rotation (which determines shear rate) and CNC concentration at 6, 9, and 12 wt%. A minimum of four layers were used to achieve coatings of 16–20 μm in thickness which could be delaminated from the PET substrate for light transmittance measurements. The maximum transmitted light intensity increases with increasing CNC ink concentration for

the 45° configuration while the 90° configuration is generally decreasing (see Supporting info, Table S4). D , calculated as the ratio of the maximum transmitted intensity between the 45° and 90° configurations, increases from 1.79 for the 6 wt% up to 4 for the 12 wt% and fixed shear rate. This suggests that preferential alignment of the crystalline domains along the shear direction is improved by increasing CNC concentration. D is maximized for the 12 wt% samples which implies that the difference in refractive index for longitudinal and transverse directions is also highest for the 12 wt% compared to the other concentrations (see Supporting info, Table S4).

An increasing order parameter as a function of gravure rotation/shear rate (Fig. 10) is observed and likely due to shear-induced alignment of the CNCs during the gravure process. At a low shear rate of 80/s, 12 wt% films show an order parameter of ~ 0.5 . As anticipated, an increase in shear rate enhances domain alignment along the shear direction, but only by a modest amount. A maximum order parameter of 0.65 is achieved at 170/s shear rate for the 12 wt%. However, a negligible reduction in the anisotropy of the CNC coating is observed at the higher gravure rotation, and the order parameter is almost constant at the elevated shear rate region. On the other hand, 9 wt% samples show less anisotropy at any gravure rotation and increasing the shear rate had a smaller effect on the domain alignment. We did not observe any anisotropic (nematic configuration) properties in

6 wt% CNC samples. Regardless, in at all concentrations, the natural chiral nematic domain structure was sufficiently disturbed to allow for high transparency.

The liquid crystal domain of the anisotropic CNC coating must align its crystal position along the shear direction during coating and the relaxation time for the CNC domain movement should be lengthy (Beck et al. 2013; Orts et al. 1998; Park et al. 2014). Thus, the initial CNC concentration contributes to alignment. A low concentration CNC suspension behaves like a Newtonian fluid and the domains show a fast relaxation time after applying shear. With enough time domains show a highly isotropic configuration (Kim et al. 2013). However, the Newtonian nature may also limit orientation in the first place. Figure S5 in the supporting information section shows the liquid crystal domains movement of 6 wt% CNC suspension along the shear direction of a doctor blade sheared specimen. Very little alignment remains after only 5 s of relaxation. At 9 wt%, it can be seen in Figure S5 that CNC domains can be aligned along the shear direction. However, in previous work, the anisotropy was completely destroyed after 5–10 min (Haywood and Davis 2017), despite having achieved 50% alignment for a 9 wt% concentration. Here, we used a 1 m/min web speed where the ink bath to drying unit distance was 50 cm, so the time before drying is 30 s. Assuming a zero time to dry once it enters the oven (while not true, we do not know the time to when the films become dry, only that they are dry when they come out), then the long relaxation time as compared to the dry time would lead to a high alignment retention, so $\sim 50\%$ anisotropy is logical considering the previous work getting similar results with simple shear. Similarly, the alignment of the 12 wt% CNC suspension has a relaxation time of 30 min (Haywood and Davis 2017), but again, is locked into place in 30 s so the even higher order parameter ($S = 0.65$) is expected figure S5 shows very little disorientation over this time scale.

Based on previous work, the 12 wt% concentration should have a higher order parameter for shear rates higher than 100/s (Haywood and Davis 2017). However, the micro-gravure surface morphology may be responsible for this effect. A standard micro-gravure with a 20π tilt angle was used for this fabrication. The shear direction was not 0° along the shear direction; hence, the CNC dispersion experiences a complex shear state and it could be expected that the CNCs

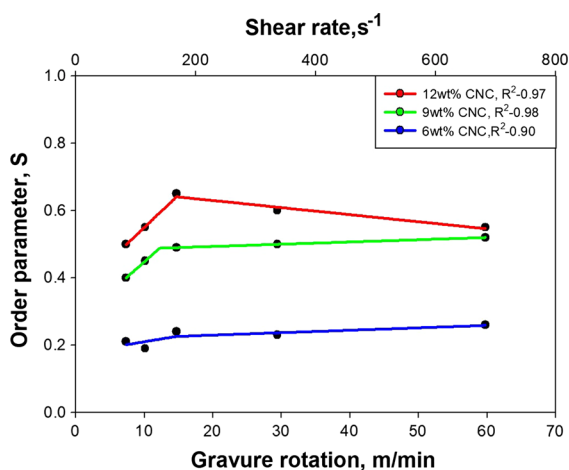


Fig. 10 Order parameter variation with roller speed (substrate speed = 1 m/min) (nonlinear regression based on a piecewise linear approximation)

should be oriented somewhere between 0° and 20° , therefore reducing the overall order parameter. An unconventional design like the 0° tilt angle micro-gravure may improve the alignment of the CNC suspension-based coating.

Conclusion

The effect of various parameters on CNC coatings for three aqueous suspensions has been described for R2R production. The effect of gravure rotation, substrate speed, and viscosity significantly control the liquid transfer mechanism from the ink bath to the flexible substrate, where the maximum coating thickness was observed at higher speed ratios for all CNC concentrations. Moreover, parameter optimization was crucial for ink transfer at the 12 wt% CNC concentration, while reduction in CNC concentration significantly reduced the necessity of parameter optimization to produce coatings.

It was noticed that the coating adhesion strength was inversely related with coating thickness. Maximum coating strength was observed for the low concentration ink system as maximum cohesive strength is attributed to a thinner coating which exhibited the lowest level of surface roughness. High concentration, high viscosity solutions exhibited qualitatively rougher surfaces which may adversely affect adhesion strength by creating weaker sites across the surface at which cracks may more easily develop.

Liquid crystal domain arrangement, quantified as the order parameter, was measured as a function of gravure rotation for various CNC concentrations. The 12 wt% CNC concentration inks retain the highest level of alignment along the gravure rotation direction, resulting in an anisotropic (nematic) coating and maximum order parameter of 0.65. However, at smaller CNC concentrations, CNC domain alignment is reduced as ink fluidity enables rapid relaxation of the aligned crystal domains. Moreover, the presence of a tilt angle (20°) in the tri-helical micro-gravure is another significant reason for crystalline domain deviation from the shear direction, which reduced the overall order parameter for CNC coating.

Acknowledgments The research was supported by the National Science Foundation Scalable Nanomanufacturing program under award CMMI-1449358. It was also partially

supported through the National Science Foundation-Integrative Graduate Education and Research Traineeship: Sustainable Electronics Grant (Grant Number 1144843).

References

- Ahn SH, Guo LJ (2008) High-speed roll-to-roll nanoimprint lithography on flexible plastic substrates. *Adv Mater* 20:2044–2049
- Bae S et al (2010) Roll-to-roll production of 30-inch graphene films for transparent electrodes. *Nat Nanotechnol* 5:574–578
- Beck S, Bouchard J, Chauve G, Berry R (2013) Controlled production of patterns in iridescent solid films of cellulose nanocrystals. *Cellulose* 20:1401–1411
- Chen S, Schueneman G, Pipes RB, Youngblood J, Moon RJ (2014) Effects of crystal orientation on cellulose nanocrystals–cellulose acetate nanocomposite fibers prepared by dry spinning. *Biomacromol* 15:3827–3835
- Chiang MY, Song R, Crosby AJ, Karim A, Chiang CK, Amis EJ (2005) Combinatorial approach to the edge delamination test for thin film reliability—adaptability and variability. *Thin Solid Films* 476:379–385
- Chindawong C, Johannsmann D (2014) An anisotropic ink based on crystalline nanocellulose: potential applications in security printing. *J Appl Polym Sci*. <https://doi.org/10.1002/app.41063>
- Chowdhury RA, Peng SX, Youngblood J (2017) Improved order parameter (alignment) determination in cellulose nanocrystal (CNC) films by a simple optical birefringence method. *Cellulose* 24:1957–1970
- Cranston ED, Gray DG (2008) Birefringence in spin-coated films containing cellulose nanocrystals. *Colloids Surf A* 325:44–51
- Diaz JA, Wu X, Martini A, Youngblood JP, Moon RJ (2013) Thermal expansion of self-organized and shear-oriented cellulose nanocrystal films. *Biomacromol* 14:2900–2908
- Diaz JA et al (2014) Thermal conductivity in nanostructured films: from single cellulose nanocrystals to bulk films. *Biomacromol* 15:4096–4101
- Dodds S, Carvalho MdS, Kumar S (2009) Stretching and slipping of liquid bridges near plates and cavities. *Phys Fluids* 21:092103
- Dodds S, Carvalho M, Kumar S (2011) Stretching liquid bridges with moving contact lines: the role of inertia. *Phys Fluids* 23:092101
- Dong H, Snyder JF (2013) Nanocellulose foam containing active ingredients. Google Patents
- Galagan Y, de Vries IG, Langen AP, Andriessen R, Verhees WJ, Veenstra SC, Kroon JM (2011) Technology development for roll-to-roll production of organic photovoltaics. *Chem Eng Process* 50:454–461
- Gardner DJ, Oporto GS, Mills R, Samir MASA (2008) Adhesion and surface issues in cellulose and nanocellulose. *J Adhes Sci Technol* 22:545–567
- Haywood AD, Davis VA (2017) Effects of liquid crystalline and shear alignment on the optical properties of cellulose nanocrystal films. *Cellulose* 24:705–716

- Hewson R, Kapur N, Gaskell P (2010) Tri-helical gravure roll coating. *Chem Eng Sci* 65:1311–1321
- Hewson R, Kapur N, Gaskell P (2011) A two-scale model for discrete cell gravure roll coating. *Chem Eng Sci* 66:3666–3674
- Huang W-X, Lee S-H, Sung HJ, Lee T-M, Kim D-S (2008) Simulation of liquid transfer between separating walls for modeling micro-gravure-offset printing. *Int J Heat Fluid Flow* 29:1436–1446
- Isogai A, Saito T, Fukuzumi H (2011) TEMPO-oxidized cellulose nanofibers. *Nanoscale* 3:71–85
- Kalia S, Kaith B, Kaur I (2011) Cellulose fibers: bio-and nanopolymer composites: green chemistry and technology. Springer, Berlin
- Kapur N (2003) A parametric study of direct gravure coating. *Chem Eng Sci* 58:2875–2882
- Kendall K (1971) The adhesion and surface energy of elastic solids. *J Phys D Appl Phys* 4:1186
- Kim J, Peretti J, Lahlil K, Boilot JP, Gacoin T (2013) Optically anisotropic thin films by shear-oriented assembly of colloidal nanorods. *Adv Mater* 25:3295–3300
- Krebs FC (2009) Polymer solar cell modules prepared using roll-to-roll methods: knife-over-edge coating, slot-die coating and screen printing. *Sol Energy Mater Sol Cells* 93:465–475
- Krebs FC, Gevorgyan SA, Alstrup J (2009) A roll-to-roll process to flexible polymer solar cells: model studies, manufacture and operational stability studies. *J Mater Chem* 19:5442–5451
- Kumar S (2015) Liquid transfer in printing processes: liquid bridges with moving contact lines. *Annu Rev Fluid Mech* 47:67–94
- Kumar V, Elfving A, Koivula H, Bousfield D, Toivakka M (2016) Roll-to-roll processed cellulose nanofiber coatings. *Ind Eng Chem Res* 55:3603–3613
- Lavoine N, Desloges I, Dufresne A, Bras J (2012) Microfibrillated cellulose—its barrier properties and applications in cellulosic materials: a review. *Carbohydr Polym* 90:735–764
- Lerouge S et al (2015) Nitrogen-rich plasma polymer coatings for biomedical applications: stability mechanical properties and adhesion under dry and wet conditions. *Plasma Process Polym* 12:882–895
- Lewis BG, Paine DC (2000) Applications and processing of transparent conducting oxides. *MRS Bulletin* 25:22–27
- Liu JC, Martin DJ, Moon RJ, Youngblood JP (2015) Enhanced thermal stability of biomedical thermoplastic polyurethane with the addition of cellulose nanocrystals. *J Appl Polym Sci*. <https://doi.org/10.1002/app.41970>
- Moon RJ, Martini A, Nairn J, Simonsen J, Youngblood J (2011) Cellulose nanomaterials review: structure, properties and nanocomposites. *Chem Soc Rev* 40:3941–3994
- Orts W, Godbout L, Marchessault R, Revol J-F (1998) Enhanced ordering of liquid crystalline suspensions of cellulose microfibrils: a small angle neutron scattering study. *Macromolecules* 31:5717–5725
- Park JH, Noh J, Schütz C, Salazar-Alvarez G, Scalia G, Bergström L, Lagerwall JP (2014) Macroscopic control of helix orientation in films dried from cholesteric liquid-crystalline cellulose nanocrystal suspensions. *ChemPhysChem* 15:1477–1484
- Patel R, Benkreira H (1991) Gravure roll coating of Newtonian liquids. *Chem Eng Sci* 46:751–756
- Peng SX, Moon RJ, Youngblood JP (2014) Design and characterization of cellulose nanocrystal-enhanced epoxy hardeners. *Green Mater* 2:193–205
- Rantanen JJ, Dimic-Misic K, Pirttiniemi J, Kuosmanen P, Maloney TC (2015) Forming and dewatering of a microfibrillated cellulose composite paper. *BioResources* 10:3492–3506
- Reising AB, Moon RJ, Youngblood JP (2012) Effect of particle alignment on mechanical properties of neat cellulose nanocrystal films. *J Sci Technol For Prod Process* 2:32–41
- Shrestha S, Diaz JA, Ghanbari S, Youngblood JP (2017) Hygroscopic swelling determination of cellulose nanocrystal (CNC) films by polarized light microscopy digital image correlation. *Biomacromolecules* 18:1482–1490
- Søndergaard RR, Hösel M, Krebs FC (2013) Roll-to-roll fabrication of large area functional organic materials. *J Polym Sci Part B Polym Phys* 51:16–34
- Wicklein B, Kocjan A, Salazar-Alvarez G, Carosio F, Camino G, Antonietti M, Bergström L (2015) Thermally insulating and fire-retardant lightweight anisotropic foams based on nanocellulose and graphene oxide. *Nat Nanotechnol* 10:277–283
- Yang X, Cranston ED (2014) Chemically cross-linked cellulose nanocrystal aerogels with shape recovery and superabsorbent properties. *Chem Mater* 26:6016–6025
- Yoo Y, Youngblood JP (2017) Tung oil wood finishes with improved weathering, durability, and scratch performance by addition of cellulose nanocrystals. *ACS Appl Mater Interfaces* 9:24936–24946
- Yoo Y, Martinez C, Youngblood JP (2017) Sustained dye release using poly (urea-urethane)/cellulose nanocrystal composite microcapsules. *Langmuir* 33:1521–1532
- Zhou Y et al (2014) Efficient recyclable organic solar cells on cellulose nanocrystal substrates with a conducting polymer top electrode deposited by film-transfer lamination. *Org Electron* 15:661–666